Meteorological Applications

RMetS Royal Meteorological Society

RESEARCH ARTICLE OPEN ACCESS

Solar and Wind Energy Variability in Tropical South America: Seasonal Ocean-Atmospheric Modulators

Nicolás Duque-Gardeazabal[1,2] | Stefan Brönnimann[1,2] | Andrew R. Friedman[1,2,3] | Edgar Dolores-Tesillos[1,2] | Olivia Martius[1,2]

[1]Oeschger Centre for Climate Change Research, University of Bern, Bern, Switzerland | [2]Institute of Geography, University of Bern, Bern, Switzerland | [3]Now at Laboratoire de Météorologie Dynamique, Institut Polytechnique de Paris, Sorbonne Université, Paris, France

Correspondence: Nicolás Duque-Gardeazabal (nicolas.duque@unibe.ch)

Received: 25 June 2025 | **Revised:** 3 December 2025 | **Accepted:** 14 February 2026

Keywords: climate oscillations | electricity | moisture convergence | moisture flux | renewable energy | solar energy

ABSTRACT

Interannual climate variability strongly influences renewable energy availability, making it a critical factor for achieving UN Sustainable Development Goals (SDGs). However, our knowledge about the potential solar and wind energy production in tropical South America and its relation to ocean-atmospheric modes of variability is limited; modes such as El Niño/Southern Oscillation (ENSO), the Atlantic Meridional Mode (AMM), among others. Therefore, we investigate the influence of these modes on solar and wind energy. We apply partial correlations and composite analyses to reanalysis and satellite data to identify the processes connecting large-scale ocean-atmospheric variability to seasonal anomalies in renewable power generation. Our study identifies three energy hubs as regions with high climatological mean energy availability: The north Caribbean (NC), eastern Brazil (EB) and western Perú/Bolivia (WPB). ENSO influences the sea level pressure (SLP) gradients, generating wind anomalies that directly affect the wind capacity factor (CF). ENSO also affects the solar CF through reduced atmospheric moisture transport and convergence, which results in fewer clouds leading to higher-than-average surface radiation or by atmospheric subsidence. ENSO impacts the NC and EB hubs, with weaker effects in the WPB hub. The AMM is associated with cross-equatorial wind anomalies that modulate wind CF, as well as moisture convergence and cloud cover, thereby influencing solar CF. Wind CF in the NC and EB hubs is inversely modulated by the AMM, weakening winds and reducing radiation over the NC and strengthening winds and increasing radiation on the EB. The Atlantic equatorial El Niño mode (Atl3) exerts minor effects, with anomalies confined to the equatorial Atlantic. Overall, we find limited complementarity between solar and wind energy at interannual time-scale. Our results provide insights for forecasting energy production and managing energy storage for periods of low renewable energy availability.

1 | Introduction

Climate variability significantly affects livelihoods by influencing renewable power systems (Bustos et al. 2017; Engeland et al. 2017). Renewable energy sources are key to achieving the UN Sustainable Development Goals, specifically through building a reliable and decarbonised energy grid (UN 2015). Both solar and wind energy production are strongly dependent on local weather conditions. Considering intra- and interannual atmospheric variability is crucial for renewable energy planning and management (Boretti and Castelletto 2020).

South America has one of the world's highest shares of renewable energy (Kieffer and López-Peña 2016). Hydropower dominates, but reliance on carbon- and gas-based facilities increases during droughts (Arango and Larsen 2010). Solar and wind energy sources are expanding (Eelsalu et al. 2024; Gil Ruiz et al. 2021; Vargas Gil et al. 2020), highlighting the need to understand their climate sensitivities.

Coupled ocean-atmospheric variability modes strongly influence the atmospheric circulation and local weather conditions in the tropics and South America, particularly at seasonal time scale (Cai et al. 2019). El Niño/Southern Oscillation (ENSO) is the most influential mode of climate variability worldwide (Timmermann et al. 2018). It strongly modulates tropical atmospheric circulation, thereby modifying near-surface wind speeds, atmospheric convergence and short-wave radiation (Cai et al. 2020). It affects renewable energy production across South America (Bianchi et al. 2022; de Perini Souza et al. 2022).

Atlantic variability modes also modulate atmospheric circulation and conditions over South America, thereby affecting renewable energy production. Moreover, they affect the hydrological cycle through changes in atmospheric water vapour circulation and convergence (Duque-Gardeazabal et al. 2025; Lopes et al. 2016; Towner et al. 2021). The Atlantic Meridional Mode (AMM) modulates the strength of the Atlantic trade winds and subtropical cloud cover (Chiang et al. 2002; Drumond et al. 2014). The Atlantic El Niño equatorial mode (Atl3) is the leading mode in the tropical Atlantic and is also associated with winds and rainfall variability (Ruiz-Barradas et al. 2000; Vallès-Casanova et al. 2020). ENSO is connected to the development of other ocean-atmospheric modes—both in the Atlantic and Indian oceans—through extratropical circulation changes and tropical atmospheric bridges (Andrian et al. 2024; Cai et al. 2019; Compo and Sardeshmukh 2010; García-Serrano et al. 2017; Martín-Rey et al. 2014). Nevertheless, the Atlantic modes are characterised by their own changes in sea surface temperature (SST) and sea level pressure (SLP), which generate distinct regional atmospheric circulation patterns (Lübbecke et al. 2018).

Other sources of variability operate at shorter or longer timescales, and thus, might modulate solar and wind energy production. These can be the Madden-Julian Oscillations (Pabón and Dorado 2008) and multi-decadal modes associated with aerosol forcing such as the Atlantic Multidecadal Oscillation (AMO) (He et al. 2023) or Interdecadal Pacific Oscillation (IPO) (Henley et al. 2015).

However, there has not been an assessment of how ENSO and the major tropical Atlantic modes jointly influence the potential solar and wind energy in tropical South America. Bianchi et al. (2022) found that ENSO, the Antarctic Oscillation and the AMO drive wind and solar energy in southern South America by changing the Atlantic circulation patterns and the moisture transport. Renewable energy sources might complement each other during energy droughts (Otero et al. 2022). Gonzalez-Salazar and Poganietz (2021) found that wind and solar energy can complement hydropower deficits during warm ENSO events using the existing generation capacity in South America. However, no studies have assessed wind-solar complementarity under Atlantic variability modes.

Therefore, our study aims to elucidate the correlations between ENSO, Atl3 and AMM ocean-atmospheric modes, and the seasonal interannual variability of potential wind and solar energy, as well as to identify the underlying physical mechanisms. Understanding these physical mechanisms can improve sub-seasonal to seasonal forecasts. Energy companies prioritise stable production to ensure a stable and reliable energy supply (Boretti and Castelletto 2020); hence, forecasts can guide mitigation strategies, including supply and storage management. We focus on ENSO, the AMM and the Atl3 because these are the dominant interannual modes of the neighbouring tropical Atlantic and Pacific basins, which most strongly modify the regional atmospheric circulation (see Section 3 methods for identification of the specific modes). We exclude the Indian Ocean modes, Madden-Julian Oscillations and multidecadal phenomena such as the AMO and IPO (see Section 5 Discussion).

Finally, we assess the wind-solar complementarity in tropical South America under each ocean-atmospheric mode (ENSO, AMM and Atl3). We exclude hydropower energy since it is strongly shaped by site-specific topographic features of the dams and reservoirs.

2 | Data

2.1 | Datasets

Meteorological reanalyses are widely used to estimate wind and solar energy production (Bloomfield et al. 2020; Cannon et al. 2015). Our study mainly relies on the ERA5 dataset, the latest ECMWF reanalysis (Hersbach et al. 2020). It provides interpolated data to a grid resolution of 0.25° and 37 pressure levels. Moreover, the hourly temporal resolution enables analysis of the diurnal cycle of wind speed, cloud cover and radiation.

Our study uses wind speed at 100 m and surface short-wave downward radiation to determine wind and solar energy capacity factors (Sections 2.2 and 2.3). Moreover, we use atmospheric circulation variables because they are related to the mechanism linking the ocean-atmospheric modes with local continental weather (Table 1). All datasets are restricted to December-1979 and November-2020 since they cover different periods. They were seasonally aggregated and analysed for each season individually (i.e., four values per year from DJF 1980 to SON 2020, later used in the analysis—Section 3 methods). The aggregation method is by seasonal average, except for precipitation, when we use the sum. As in other studies, we assume that meteorological conditions at the location of energy installations are adequately represented by ERA5 grid box values.

Focusing on wind resources, Gualtieri (2022) evaluated ERA5 and other reanalyses and concluded that ERA5 is reliable in offshore and flat onshore areas. Gil Ruiz et al. (2021) reported close agreement between wind energy production estimated with ERA5 and observations over northern South America, using the intensity-duration-frequency distributions for the estimation.

Solar radiation estimated by reanalysis generally shows a positive bias of ERA5 compared to observations (Kies et al. 2021; Wilczak et al. 2024), especially in tropical regions and South America. Nevertheless, temporal correlations are mostly above 0.9, with minima near 0.8 (Ramirez Camargo and Schmidt 2020);

TABLE 1 | Datasets and variables used in our study.

Source	Variable	Temporal resolution	Spatial resolution
ERA5—reanalysis Hersbach et al. (2020)	Wind speed at 100 m	Hourly	0.25°
	Sea level pressure (SLP)		
	Vertically integrated water vapour flux (VIMF)		
	Vertically integrated moisture divergence (MDiv)		
	Surface short-wave downward radiation		
	2 m temperature		
MSWEP Beck et al. (2019) Gauge, satellite and reanalysis	Precipitation	Monthly	0.1°
EUMETSAT—CLARA A3 Karlsson et al. (2023) Satellite	Cloud cover fraction	Monthly	0.25°
ERSSTv5 Huang et al. (2017) Ships, buoys and floats	Sea surface temperature (SST)	Monthly	2°

ERA5 underestimates short-wave radiation in clear-sky conditions (Sianturi et al. 2020).

Sea surface temperature anomalies (SSTA) are used to identify the key ocean-atmospheric modes (Section 3.1). We use SSTAs from the Extended Reconstructed SST dataset version 5 (Huang et al. 2017).

Cloud cover is expected to influence the surface downward shortwave radiation. We use vertically integrated water vapour flux components (also known as vertically integrated moisture flux, VIMF) and the vertically integrated moisture divergence (MDiv) from ERA5, the latter related to cloud cover. We also used the satellite-based EUMETSAT CLARA-A3 cloud cover area fraction (Karlsson et al. 2023) to verify the dynamics in several sources of information. Precipitation data comes from the Multi-Source Weighted-Ensemble Precipitation v2.8 (MSWEP) (Beck et al. 2019); this dataset integrates rain gauges, satellite and reanalysis data.

2.2 | Wind Capacity Factor

The wind capacity factor (CF) represents the ratio between actual and maximum possible energy production of a wind turbine that operates at rated power (Bloomfield et al. 2022). We estimate the wind CF at 100 m—the typical height of wind turbines—because it provides a dimensionless energy variable comparable to other energy sources, such as solar. Other wind energy variables, such as the wind power density (WPD), are more suitable for comparing different locations without assuming specific turbines (Antonini et al. 2024), but comparing WPD with solar energy requires assuming transformation coefficients (WPD was also calculated but is not shown). The wind CF is calculated from ERA5 wind fields using the power curve from the assumed Vestas V117–3.45 turbine (used in similar regional studies; Gil Ruiz et al. 2021; Wind-turbine-models 2025), dividing the power output by its rated power of 3450 kW. Our method excludes the wake effects induced by surrounding turbines and grid-induced curtailment since detailed information on current and planned energy facilities is not consistently available region-wide (Dolores-Tesillos et al. 2025). Given that our aim is to estimate the interannual variability and its associated modulators, we interpret the estimated wind CF as potential wind energy.

As the wind CF depends on the cube of the wind speed, calculating it at different time steps yields different distributions. Therefore, we use hourly fields from ERA5—the finest publicly available resolution—and afterwards aggregate the hourly CF to seasonal means for the posterior analysis. SLP is expected to influence wind components; hence, we use SLP from ERA5 to study the modulation mechanisms of the ocean-atmospheric modes (Table 1).

2.3 | Solar Capacity Factor

Photovoltaic modules (PV) have a wide range of different panels whose efficiency is affected by temperature and surface solar radiation (Evans and Florschuetz 1977). We analyse the solar capacity factor (CF), which enables site comparison without specifying the type of solar panel or the characteristics of current and future energy facilities. Bett and Thornton (2016) presented an empirical relationship for calculating the solar CF that estimates the cell efficiency from the downward surface solar radiation, the module temperature and the irradiance at standard test conditions (STC) ($G_{stc} = 1000\,W/m^2$) (see appendix of Bett and Thornton 2016). The module temperature considers 2 m air temperature and the surface downward short-wave radiation to establish the working efficiency of the panel. The higher the ambient and module temperature, the lower the panel efficiency.

Our study then uses hourly fields of solar radiation and air temperature from ERA5. The potential solar CF is then filtered to only daytime and aggregated to seasonal averages, the latter consistent with the wind CF methodology.

3 | Methods

We first mapped the multiannual availability of solar and wind energy to identify regions of high potential for renewable energy production, hereafter referred to as 'energy hubs'. Second, we identify the seasonal ocean-atmospheric variability modes that are statistically associated with the wind and solar capacity factors (Section 3.1), and analyse the underlying physical mechanisms behind these associations using composite analysis (Section 3.2). Third, we assess the complementarity between both sources of energy (Section 3.3).

Results are presented in Section 4, where we first identify the energy hubs (Section 4.1), then detail the influence of the ocean-atmospheric modes on these regions (Sections 4.2 and 4.3) and finally assess how the modes modulate energy complementarity (Section 4.4). We conclude with a discussion of the broader implications of these relationships.

3.1 | Modes of Variability

Our study identifies coupled ocean-atmospheric modes with SSTA indices. SSTA are detrended with a regression with de-seasonalised CO_2 concentrations ($R^2 = 0.92$, $p < 0.001$) (Thoning et al. 1989) to focus on interannual variability and exclude the effect of global warming. Principal component analysis is applied to detrended SSTs in the Atlantic and Pacific oceans to extract dominant ocean-atmospheric modes. Other ocean basins that are not close to the study area were excluded because their teleconnections are closely related to those exerted by ENSO (Cai et al. 2019) (see correlations analysis below). PCA loadings are used to define spatial boxes, from which box-averaged climatic indices are built (boxes boundaries were consistent with the literature review, Fernandes et al. 2015; Vallès-Casanova et al. 2020). Hence, our study defines the Atlantic indices as:

- The AMM monthly index is defined as the difference between the spatially averaged northern tropical Atlantic SSTA [70° W–15° W, 5° N–25° N] and southern tropical Atlantic SSTA [40° W–0° W, 25° S–5° S].
- The Atl3 monthly index is identified as the spatial average of eastern equatorial Atlantic SSTA [20° W–0° W, 3° S–3° N].

To analyse ENSO, we calculate the El Niño Longitude Index (ELI) because it considers the diversity of east- and central-Pacific ENSO events (Williams and Patricola 2018). This index represents the decomposition of tropical Pacific variability better than fixed box-average indices, which is important for the variability of tropical convection. High ELI values correspond to warm central/eastern Pacific SSTAs (El Niño), whereas low values indicate cold anomalies (La Niña). Time series of the indices and PCA loadings are shown in Figure S1.

To map the impacts of the modes, we compute partial correlation between the three indices (ELI, AMM, Atl3) and the wind and solar CF at each grid point. Removing the simultaneous confounding effects from other modes (Y and Z) indicates the relation of mode X with the analysed variable. We also show the results for the energy hubs. Partial correlations with other indices different from the ELI, AMM and the Atl3 were performed but are not shown since their teleconnections are closely related to ENSO (Cai et al. 2019).

3.2 | Identifying the Physical Mechanisms of the Teleconnection

We establish the physical processes of the connection through anomaly composite analysis (mean of anomaly fields at specific times; Arias et al. 2020; Vallès-Casanova et al. 2020). The composites are defined based on the seasonally averaged values of the SST indices (indices time series in Figure S1); when values exceed ±1 standard deviation from the mean—for the given season distribution, e.g., boreal summer—the mode is considered to be in its positive or negative phase, respectively. For the ELI, the threshold is set to ±0.75 standard deviations to align with the Oceanic El Niño Index events.

Composites are built with the variables influencing wind speed and radiation (i.e., SLP, winds, VIMF, MDiv and cloud cover). Composites are always compared to the neutral phase (defined when indices' values are within the previous thresholds). The composites' statistical significance is estimated with a two-sample Student's *t*-test.

El Niño—ENSO positive warm phase—develops in the boreal summer (JJA, June to August, by the initial letters of the months), grows from September to November (SON) and peaks in boreal winter D(0)JF(+1) (Timmermann et al. 2018). Conversely, the Atl3 mode peaks in JJA and the AMM can be active year-round, but it is strongest in boreal spring (MAM) (Ruiz-Barradas et al. 2000; Vallès-Casanova et al. 2020). Accordingly, we focus the ENSO analysis on SON and DJF, and the Atlantic modes on MAM and JJA.

3.3 | Complementarity of Wind and Solar Energy

We assess the complementarity of both energy sources by comparing their standardised anomalies under the influence of each mode. This is at the time steps of the previous composite analysis. The energy hubs are collocated regions with high multiannual potential CF, identified in our first analysis (Section 4.1). Complementarity is assessed between hubs paired geographically (shortest centroids distance between solar hub and wind hub) to reflect realistic integration potential within regional grids. Complementarity between distant hubs is not considered practical or even possible.

Two scales of complementarity are evaluated. First, a multiannual mean complementarity seeks to assess differences in the

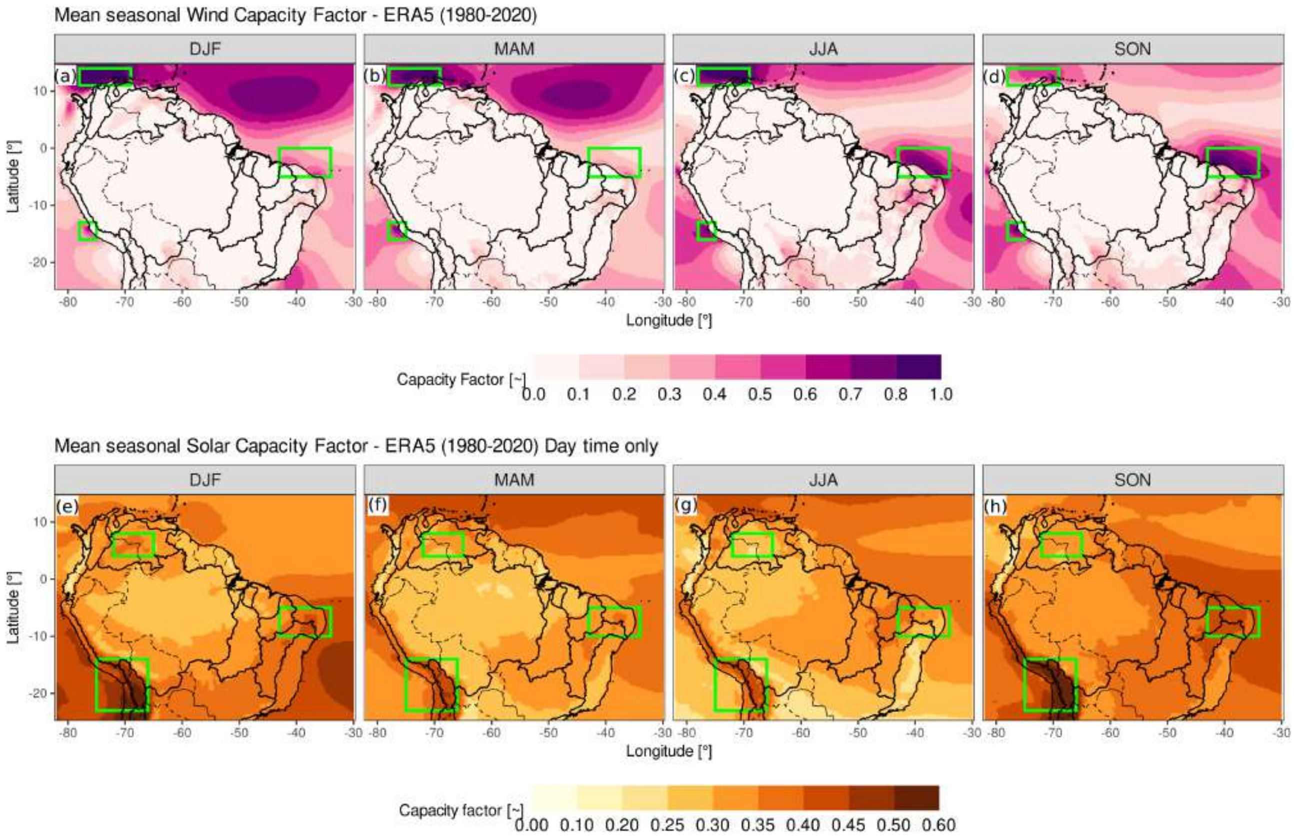

FIGURE 1 | (a–d) Multi-annual mean seasonal wind CF at 100 m above ground. (e–h) multi-annual mean seasonal daytime solar CF. Green rectangles highlight the regions with the highest potential wind and solar CF considering all seasons (energy hubs). Black continuous lines are river basins; dashed lines are country borders. Titles of panels refer to the first letters of the months in each season, that is December to February for panels (a, e).

climatological seasonal cycles of the solar and wind CF. Second, an interannual complementarity is based on the variability modes exert over the renewable energy. It compares composites across energy sources, phases of the modes (negative, neutral and positive) and for each season and hub individually. We also quantify complementarity with Spearman correlation since it handles skewed distributions (e.g., wind CF) and extreme events better than Pearson correlation.

4 | Results

4.1 | Identifying Renewable Energy Hubs and Their Seasonal Variability

We identified three key regions based on the 1980–2020 mean seasonal wind CF (Figure 1a–d), and also three with high solar CF (Figure 1e–h). We then grouped them into three paired energy hubs (Table 2), since all have another region with high potential from the opposite sources close to them.

Wind hubs are located in coastal/oceanic areas. Two hubs have a CF value exceeding 0.6 in at least two seasons (North Caribbean and Southwestern Perú) (Figure 1a–d). The Caribbean coast shows nearly year-round high wind resource, which attenuates in SON when the Intertropical Convergence Zone (ITCZ) moves northward. The northeastern Brazilian coast has a long strip

TABLE 2 | Energy hubs classified by proximity of wind and solar resources.

Energy hub	Wind	Solar
#1 Northern Caribbean hub	Caribbean coast	Orinoco savannas
#2 Eastern Brazil hub	Northeastern Brazil coast	Eastern Brazil
#3 Western Perú/ Bolivia hub	Southwestern Peruvian coast	Bolivian altiplano

that exceeds 0.6 in JJA and SON but is weaker in other seasons (Figure 1c,d). Low wind CF values over the ocean also move with the annual solar cycle and the ITCZ.

The solar CF exhibits a significant annual cycle (Figure 1e–h) also linked to the annual migration of the ITCZ. Three high solar CF regions are located in the north, east and west of tropical South America, close to wind hubs (Figure 1a–d). For eastern Brazil and the Bolivian Altiplano in the southwest, the solar CF exceeds 0.4 in at least three seasons, whereas the Orinoco savannas in the northern hub, the CF is higher than 0.35 in DJF but drops to 0.2 in JJA. The Bolivian altiplano in the Western hub shows a substantial seasonal cycle, with values higher than 0.5 in SON and lower than 0.35 in JJA. Table 2 presents

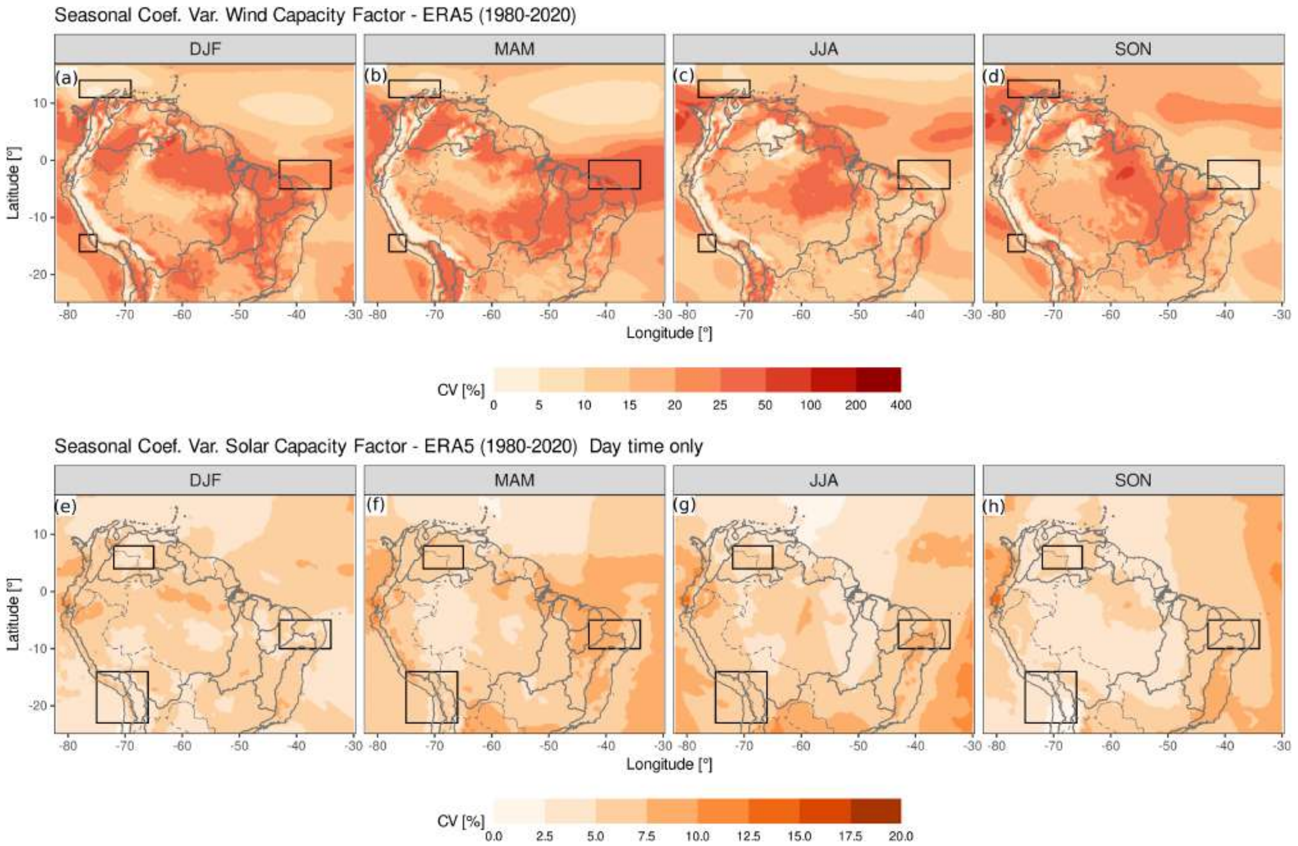

FIGURE 2 | Coefficient of variation (CV) for (a–d) wind CF for each season and (e–h) daytime-only solar CF for each season. Black rectangles are the same energy hubs as in Figure 1.

the identified high potential renewable energy regions (energy hubs, Figure 1).

Energy companies seek low variability to ensure a stable and predictable energy supply (Boretti and Castelletto 2020). We estimate the CF variability with the coefficient of variation (ratio of the standard deviation and mean, $CV = \sigma/\mu$) and afterwards we look for phenomena modulating that variability which could aid in its prediction (see Sections 4.2 and 4.3).

Wind CF interannual variability of seasonal estimates is generally below 25% over the oceans but higher over the continent (Figure 2a–d), due to surface friction of wind with topography, which imposes shear stress and turbulence, in turn reducing momentum and wind speed. Conversely, the northern Caribbean and the Peruvian hubs remain relatively stable with a CV bigger than 15% in only one of the seasons (SON and DJF, respectively). The northeastern Brazil hub reaches ca. 25% in MAM when the ITCZ variability strongly affects the wind speeds.

The solar CF reflects the cloud-radiances assimilated data from polar orbiting satellites (Figure 2e–h), where some swaths have a slightly higher variability, for example over the Caribbean and northeast Brazil in JJA (Figure 2g). However, almost everywhere the CV is below 10% and just over northeast Brazil and the northwestern coast reaches a higher variability; none of the solar hubs reach a coefficient of variation higher than 10%. The CV is below 7% in all seasons over the western Bolivian solar hub due to the high-altitude topography and low atmospheric moisture which give this hub a special geographical advantage for solar energy. Solar CF variability is, in general, lower than wind CF variability.

4.2 | Ocean-Atmospheric Oscillations Associated With the Variability of the Energy Hubs

Ocean-atmospheric modes influence wind speed across most of the study domain and, therefore, also the wind CF in the identified energy hubs (Figure 3). The magnitude of the correlations changes geographically and seasonally (Figure S2 for correlation maps, see also Section 5).

The wind CF is positively correlated with ENSO over the northern hub during its growing phase (from June to the DJF peak, Figure 3c,d) and with the eastern wind hub in MAM and JJA. The western hub is affected by ENSO in DJF (Figure 3i). The AMM is associated with a seesaw effect over the north coastline and eastern Brazil hub (negative correlation for the northern and positive for the eastern hub, Figure 3c,d,g,h). This effect is observed year-round but is strongest between March and November. The western hub correlates with the AMM, but because this mode is associated with the Atlantic basin thermodynamics, these relationships might be spurious (physical mechanisms in Section 4.3). In contrast, the Atl3 shows limited influence on the wind CF (Figure S2). Its main signal occurs in MAM over the

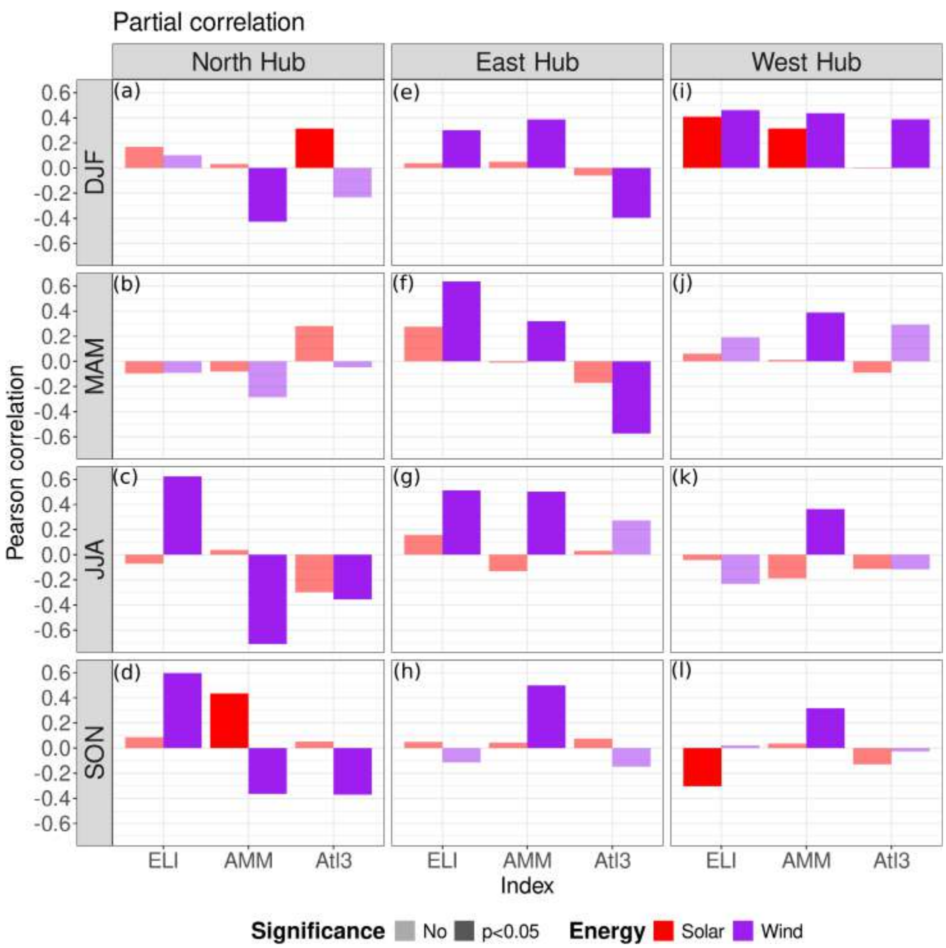

FIGURE 3 | Pearson partial correlations between the ocean-atmospheric modes of variability and the solar and wind CF, classified by season and by energy hub. Panels (a–d) show correlations for the northern hub, (e–h) for the eastern and (i–l) for the southern hub. Panels (a, e and i) are for season DJF and so on for the other seasons.

tropical western Atlantic, a region also affected by ENSO and the AMM but with opposite sign. Significant correlations between the Atl3 and the northern hub might also be spurious (see Section 5 Discussion).

The influence of ocean-atmospheric modes on the solar CF is more localised over land and also weaker over the energy hubs (Figures 3 and S3). ENSO affects eastern and northwestern South America (Figure 3a,f,i), with the largest affected area during DJF (Figure S3), consistent with the well-documented influence over the continent and the Amazon basin. The AMM also produces a seesaw effect—same as with the wind CF—between the eastern equatorial continent and the Caribbean coast; the impacts change depending on the season (Figure 3a–d). In MAM, the AMM modulates radiation over eastern Amazonia, migrating to the central Amazon in JJA (Figure S3). In SON, it modulates radiation over the Orinoco savannas and western Amazon, affecting the northern solar hub (Figures 3d and S3). ENSO is the only mode that affects the Bolivian solar hub, particularly in DJF and SON (Figure 3i,l). The correlation between the solar western hub and the AMM might be spurious. The Atl3 influences radiation over the equatorial Atlantic and with impacts concentrated over eastern South America (Figure S3).

The correlations of the Atl3 with the wind and solar CF are less widespread than those from ENSO and the AMM. It rarely influences any of the energy hubs (Figures S2 and S3).

4.3 | Physical Mechanisms Associated With the Energy Variability

Figure 4 shows the wind CF anomaly composites associated with ENSO phases. Wind vectors represent anomalies relative to the multi-annual mean; vectors pointing opposite to the mean wind direction indicate a reduction in absolute wind speed and thus in wind CF.

During El Niño, anomalously warm SSTs and low SLP develop over the central and eastern equatorial Pacific (JJA to DJF). The reduced SLP strengthens the easterly trade winds from the Caribbean to the South Pacific in SON and DJF (Figure 4a,c), boosting the wind CF over the northern wind hub and the southwestern Perú. Composites for MAM and JJA are shown in Figure S4; JJA shows patterns similar to SON while the northward anomalies in MAM resemble the positive phase of the AMM (Figure 5a; see Section 5 discussion). El Niño also promotes anomalous descending motion over the

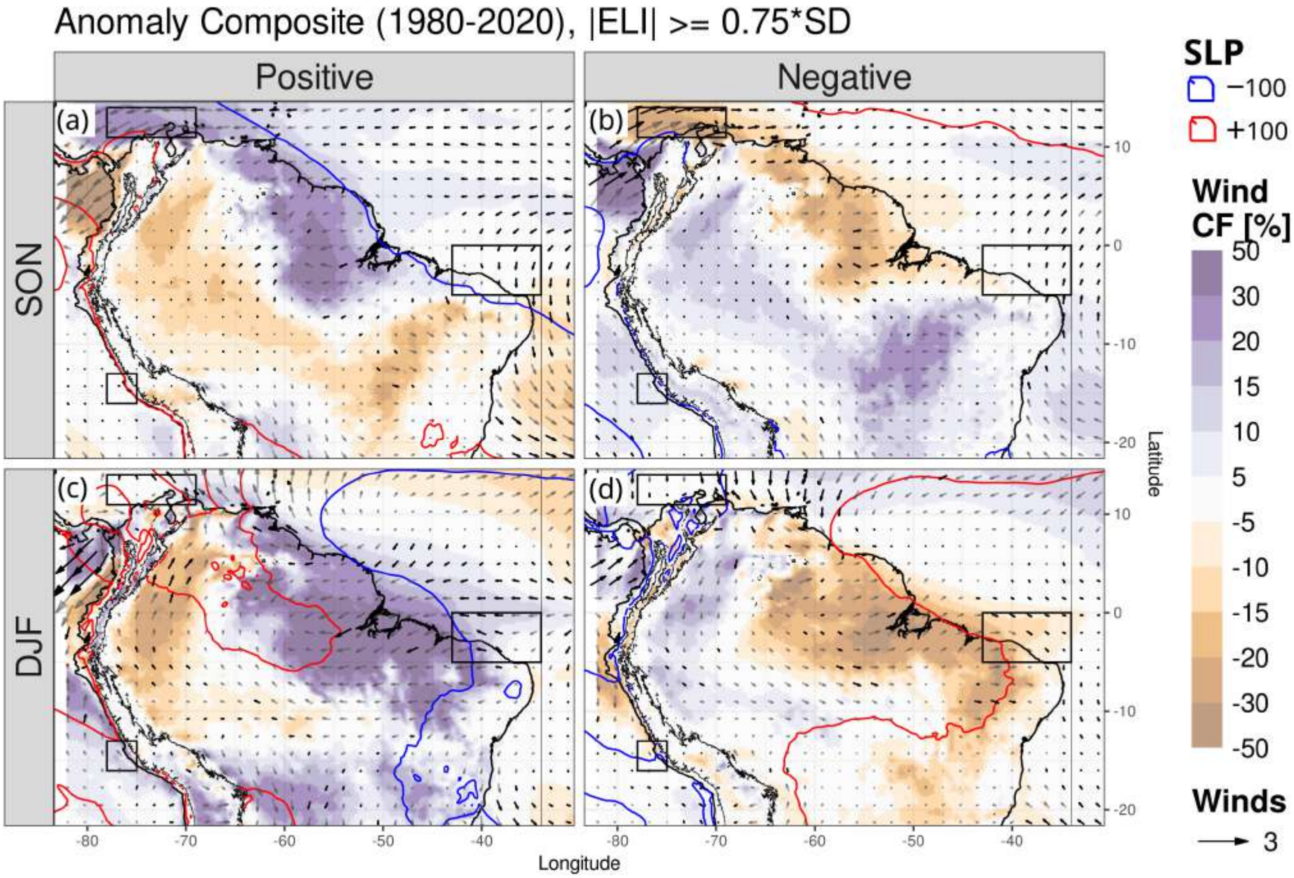

FIGURE 4 | Anomaly composite—during both phases of ENSO—of wind CF (shadings), sea level pressure (SLP, contours every 100 Pa, negative in red, positive in blue) and 100 m wind (arrows). SLP was masked on terrain above 1000 m.a.s.l. (mask depicted with black thin lines). Wind anomalies are depicted in black where the difference from the neutral phase is statistically significant at 95% confidence level, and in grey otherwise. Panels (a, c) correspond to the positive and (b, d) for the negative. Panels (a, b) show SON and (c, d) DJF. Wind hubs are outlined with black boxes, as in Figure 1a–d.

western equatorial Atlantic—especially in DJF—through an atmospheric bridge (Cai et al. 2020). This strongly increases SLP over the Atlantic and accelerates the easterly trade winds (Figure 4c), rising wind CF at the eastern hub. During La Niña, the stronger SLP and winds over the eastern Pacific in SON weaken the Caribbean trade winds (Figure 4b), decreasing wind CF in the northern hub. In DJF, La Niña increases convergence and rainfall over the Amazon and northeastern Brazil, accompanied by a slight SLP decrease over the continent (Figure 4d), reducing wind CF speed in the western equatorial Atlantic.

The AMM is associated with opposing SST and SLP anomalies between the tropical North and South Atlantic (Chiang et al. 2002). It generates cross-equatorial wind anomalies, most active between February and August, that accelerate or decelerate wind speeds (Figure 5). In its positive phase, negative SLP anomalies in the northern Atlantic and positive anomalies in the southern Atlantic are associated with northward wind anomalies. This enhances wind CF over northeast Brazil (Figure 5a,c), whereas the weakened northeasterly trade winds result in reduced wind CF over the northern Caribbean hub. The negative phase causes the opposite and redirects wind southward (Figure 5b,d), with stronger influences in JJA, whereas the positive phase dominates in MAM. There are some differences in other seasons such as a clear influence in SON in the northern hub but not in the east hub (Figure S5). AMM-related changes in wind CF over southwestern Peru are likely driven by other processes, as this mode is not linked to significant eastern Pacific SLP anomalies (see Section 5 discussion). Overall, the AMM inversely modulates wind CF between the Caribbean and northeast Brazil hubs.

The Atl3, in its positive phase, features warm SSTs and low SLP in the eastern equatorial Atlantic (Figure S6, JJA), weakening trade winds, depicted as westerly wind anomalies. These anomalies exert minimal influence on wind CF, since circulation changes remain largely confined to the eastern equatorial Atlantic. Stronger Easterlies in the Atl3 negative phase are associated with El Niño (see Section 5 Discussion). Atl3 effects on wind CF over the energy hubs or the continent remain modest.

Notably, in boreal spring (MAM), the AMM and Atl3 generate similar but opposite-signed atmospheric circulation anomalies (see the positive phase of the AMM and the negative phase of the Atl3, Figure 5a vs. Figiure S6). This is associated with the connection between the two modes (see Section 5 Discussion).

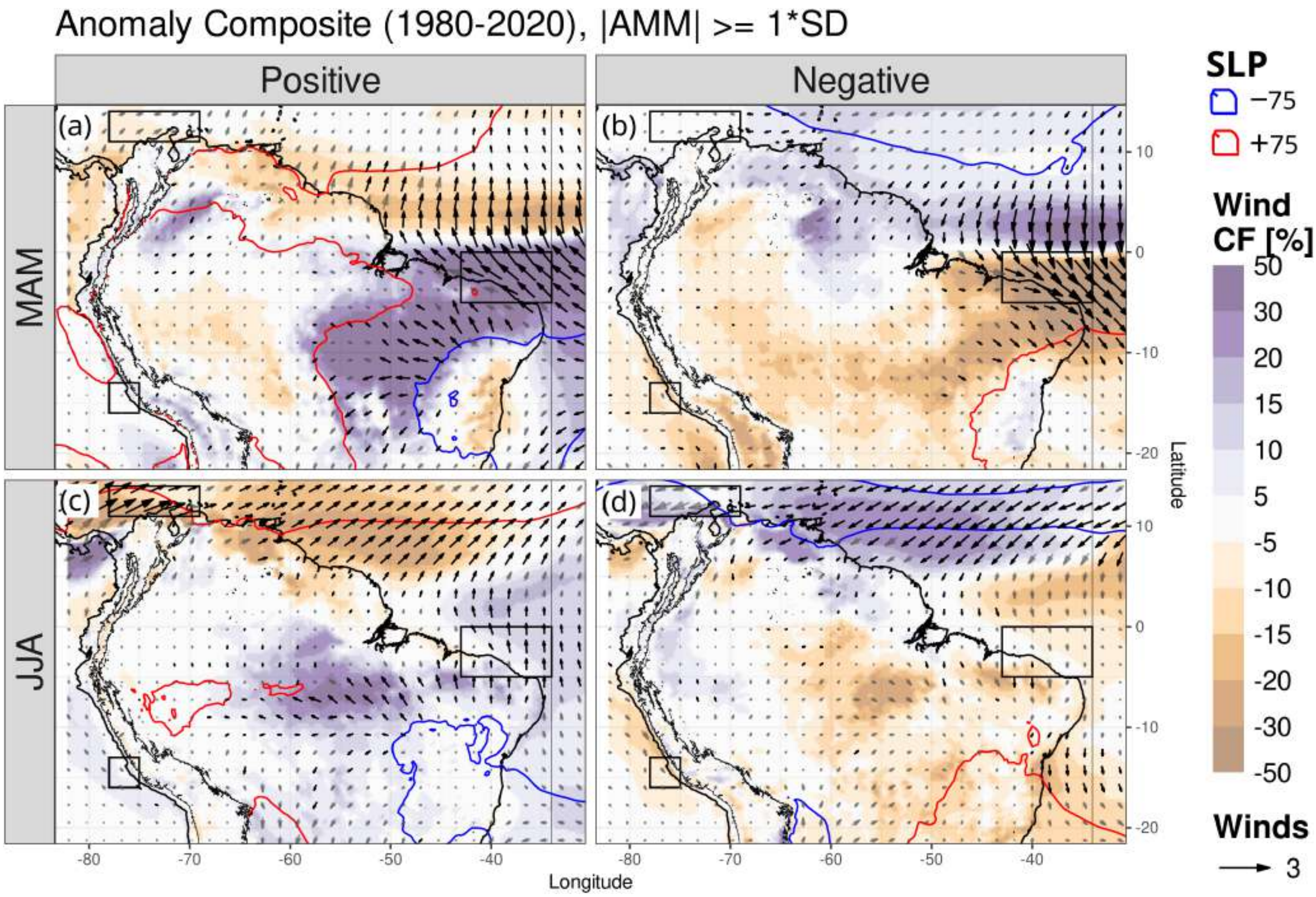

FIGURE 5 | As in Figure 4, but for the positive and negative phases of the AMM. SLP contours are at 75 Pa intervals.

Regarding the solar CF, El Niño is associated with suppressed convection over eastern South America via atmospheric subsidence, which reduces cloud cover and increases surface solar radiation (Figure 6). In northwestern South America, weaker low-level winds decrease moisture advection and convergence (Figure 6a,c), further reducing clouds and increasing solar CF (Figure 6e,g). However, the northern solar hub shows modest CF changes. An exception unfolds over the Orinoco lowlands in MAM, when increased moisture advection and convergence generate more clouds, reducing the solar CF (Figure S7); this is related to Caribbean SLP dynamics (Figure S4). Increased solar CF over the western Bolivian hub in the DJF-positive phase might be associated with the stronger northerly winds along the Andes, advecting moisture southward to Argentina (Figure 6c,g); moisture that does not climb the Andes eastern slope, resulting in reduced cloud cover over the hub. Conversely, La Niña phase intensifies Amazonian and northwestern convergence and cloudiness, reducing the solar CF but only notably in the northern hub (bigger than 2%, Figure 6h). Moreover, there are asymmetric responses between phases, for example the eastern hub is just affected in El Niño phase in DJF (Figure 6g). Cloud cover anomalies—and hence in solar energy—seasonally change location with the position of the ITCZ. Agreement across gauge-satellite precipitation, satellite cloud cover and reanalysed moisture convergence supports the robustness of these mechanisms.

The AMM influences solar radiation through meridional moisture advection, anomalous moisture convergence and clouds, thereby affecting the solar CF (Figure 7). For MAM positive phase, northward advection enhances convergence, cloud cover and is associated with less radiation over northern South America, diminishing the solar CF in the northern hub (Figure 7a,e). Simultaneously, displaced moisture generates divergence near the equatorial east, reduces clouds and increases radiation, though this does not extend into the eastern hub (Figure 7a,e). This mechanism differs from that exerted by ENSO—downward atmospheric movement. Conversely, in the negative phase, southward moisture advection from the Atlantic is associated with increased moisture convergence and cloud cover, which affects the eastern solar hub (Figure 7b,f). These effects are asymmetric across phases. Moreover, in JJA, the anomalies in convergence move towards the northern Amazon, but solar hubs are not significantly affected (Figure 7c,d,g,h). However, in SON, Caribbean moisture advection modulates solar CF in the Orinoco hub (Figure S8). The western Bolivian hub is apparently unaffected by the AMM, likely due to its distance from the Atlantic atmospheric circulation changes. Across seasons, AMM-related solar CF anomalies migrate westward, from eastern Brazil in DJF and MAM, to the central Amazon in JJA and towards the Andes in SON (Figures 7 and S8).

Regarding the Atl3 (Figure S9), it only exerts weak influence on the solar CF in JJA when reduced SLP over the equatorial east Atlantic increases moisture convergence and clouds over eastern South America. Conversely, the JJA negative phase is associated with reduced cloud cover and increased solar CF due to strengthened easterly winds, often coinciding with Pacific El Niño conditions (see Section 5).

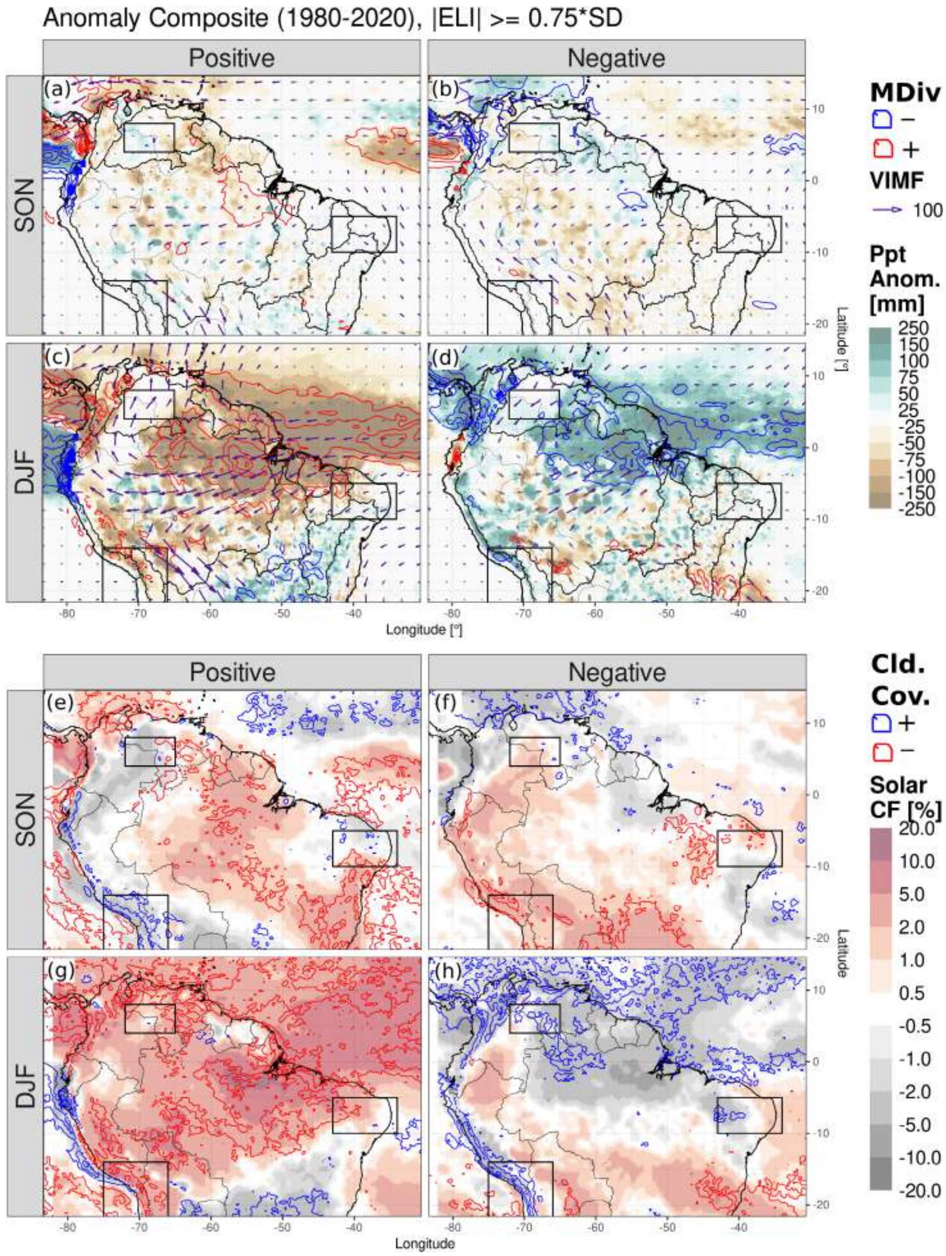

FIGURE 6 | (a–d) Anomaly composite—in the two phases of ENSO—of vertically integrated water vapour flux components (VIMF; arrows depicted in aquamarine where the difference with the neutral phase is statistically significant at 90% confidence level, and in grey otherwise), moisture divergence anomalies (MDiv; contours at 3 kg/m^2 intervals; positive in red, negative in blue) and MSWEP precipitation (shading). (e–h) Solar capacity factor (CF, shading) and satellite cloud cover fraction (contours at 4% intervals; negative in red, positive in blue). Panels (a, c, e, g) correspond to El Niño phase and (b, d, f, h) to La Niña phase. Panels (a, b, e, f) show SON and (c, d, g, h) show DJF. Solar energy hubs are outlined with black boxes, as in Figure 1e–h.

In both ENSO and AMM cases, solar CF anomalies are consistent with satellite cloud cover changes (Figures 6 and 7), reinforcing the physical basis of these relationships.

4.4 | Complementarity Between Solar and Wind Resources

Planning the construction and the grid interconnection of power plants depends on both multi-annual availability and the annual cycle of solar or wind resources (Figure 1). Table 3 shows that each hub experiences at least one season when both wind and solar CF fall below the multi-annual mean. For instance, in SON the northern hub wind CF is 0.22 below average, while the solar CF is slightly above average (+0.01). In MAM, both the eastern and western hubs experience simultaneous reductions in both energy sources, hampering complementarity. Conversely, each hub also has at least one season when one energy source increases while the other decreases (i.e., they partially complement each other); these are JJA for the north hub, DJF for the east and west hubs.

Considering the ocean-atmospheric variability modes is essential for anticipating seasonal energy availability and

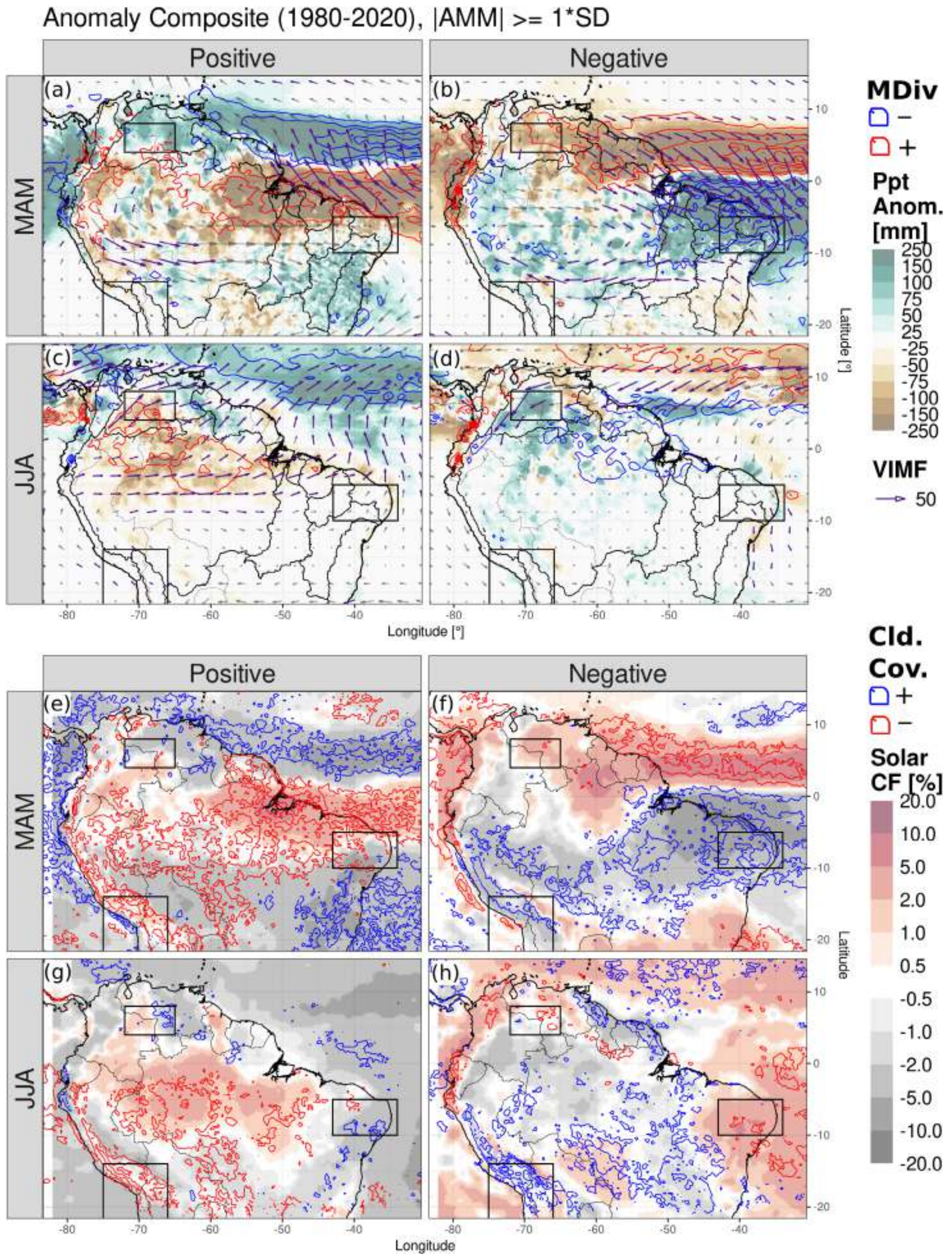

FIGURE 7 | As in Figure 6, but for the positive and negative phases of the Atlantic Meridional Mode (AMM) in MAM (a, b, e, f) and JJA (c, d, g, h).

operations. ENSO does not considerably enhance or reduce complementarity; its effects depend on hub location and season (Figure 8). In the northern hub, ENSO phases influence energy towards the same anomaly sign in DJF and MAM, with a clear decrease in MAM during the positive phase (Figure 8a,d). Whereas in JJA and SON, solar and wind anomalies diverge, providing some seasonal complementarity (Figure 8g,j). In the eastern energy hub (Figure 8b,e,h,k), complementarity is virtually non-existent independent of the analysed ENSO phase because both energy sources move in the same direction. Fortunately, El Niño generates positive anomalies, which could offset the hydropower deficits that Brazil typically experiences during these events (Gonzalez-Salazar and Poganietz 2021). The western hub shows a similar pattern: little to no complementarity in most seasons and ENSO phases (Figure 8c,f,i,l). Sub-distribution variability is large, as reflected in wide error bars.

The AMM is also associated with non-complementary anomalies in many seasons and phases. However, the AMM generates more opportunities for complementarity than ENSO (Figure 9). For the northern hub, opposite-sign anomalies emerge during DJF negative phase and in SON (Figure 9a,j). In MAM, complementarity is weak to non-existent, with high variability (Figure 9d). In JJA, AMM affects wind CF but not solar CF, limiting complementarity (Figure 9g, ITCZ over northern South America in JJA). In the eastern hub, complementarity arises in JJA and SON positive phases (Figure 9h,k), whereas in DJF and MAM, both sources respond similarly (Figure 9b,e). In the western hub, the AMM positive phases produce complementary anomalies in JJA and SON, but the other seasons and phases do not (Figure 9i,l). As with ENSO, variability across composites is large and asymmetries between AMM phases are common (i.e., one phase reports complementarity, but in the other phase, both energy sources do not complement each other, see Figure 9b,e).

TABLE 3 | Multi-annual mean renewable energy capacity factors.

Hub							
Season	**Energy**	**#1**	**Northern**	**#2**	**Eastern**	**#3**	**Western**
DJF	Wind	0.78	(0.11) [17%]	0.3	*(−0.11) [−26%]*	0.29	*(−0.10) [−25%]*
	Solar	0.34	(0.03) [10%]	0.39	*(0.02) [5%]*	0.45	*(0.05) [11%]*
MAM	Wind	0.70	(0.04) [6%]	0.2	**(−0.21) [−50%]**	0.38	**(−0.01) [−2%]**
	Solar	0.31	(0.00) [0.00%]	0.34	**(−0.03) [−7%]**	0.37	**(−0.03) [−8%]**
JJA	Wind	0.74	*(0.07) [11%]*	0.52	*(0.11) [28%]*	0.46	*(0.06) [16%]*
	Solar	0.27	*(−0.04) [−12%]*	0.32	*(−0.04) [−12%]*	0.34	*(−0.07) [−17%]*
SON	Wind	0.44	**(−0.22) [−34%]**	0.61	(0.20) [48%]	0.43	(0.04) [11%]
	Solar	0.32	**(0.01) [2%]**	0.42	(0.05) [13%]	0.46	(0.06) [14%]
Annual	Wind	0.67		0.41		0.39	
	Solar	0.31		0.37		0.41	

Note: Values represent area-average over the energy hubs defined in Figure 1 and Table 2. Values in parentheses show the seasonal difference from the annual long-term mean and in brackets give the relative percentage with respect to that mean. Values in bold indicate seasons when both sources decrease, whereas italics highlight seasons when one source substantially increases as the other decreases (complementarity).

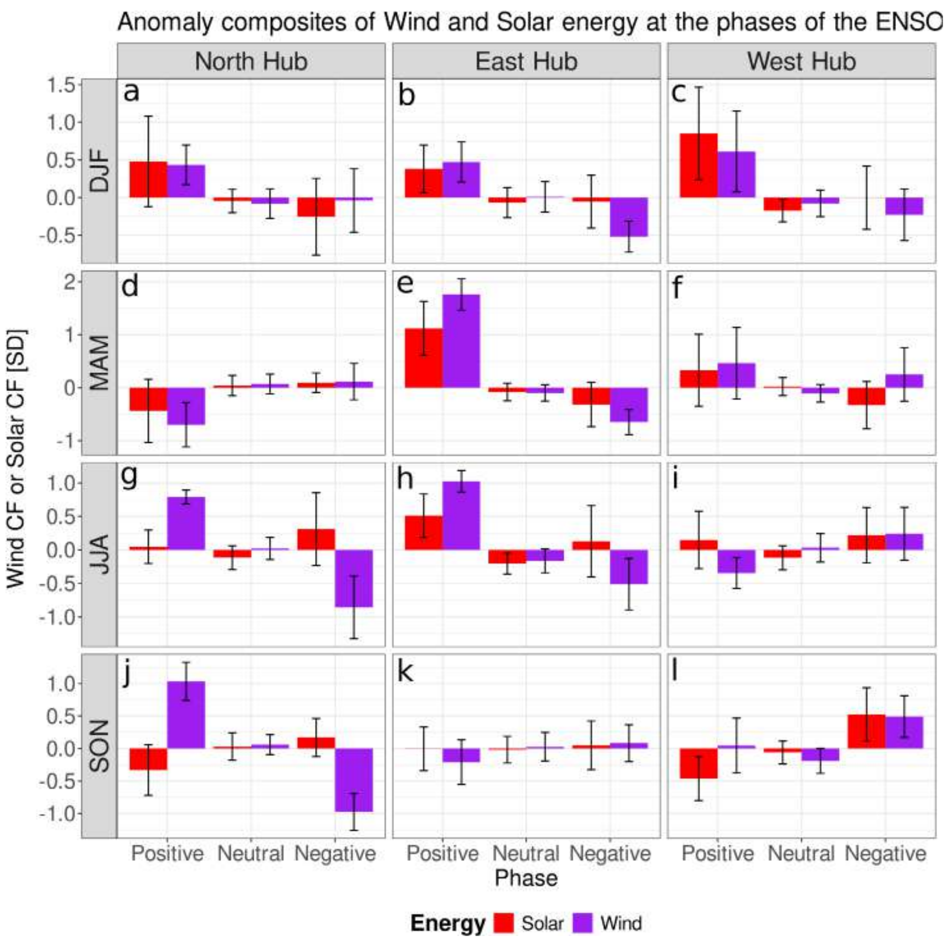

FIGURE 8 | Average wind and solar CF anomaly composites for the three phases of ENSO (positive, neutral and negative), grouped by season and by energy hub. All anomalies are expressed in standard deviations. Panels (a, d, g, j) depict the northern hub, (b, e, h, k) the eastern hub and (c, f, i, l) the western hub. Panels (a–c) correspond to DJF, and so on for the other seasons. Whiskers indicate the standard error of the composites.

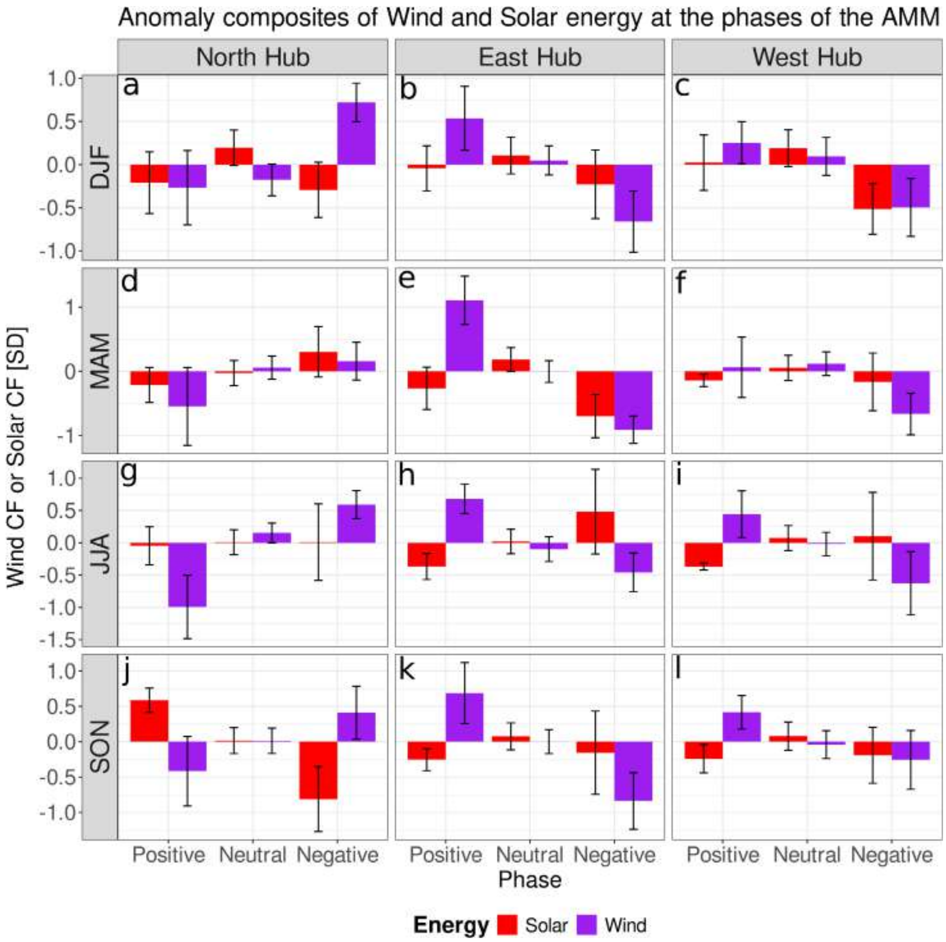

FIGURE 9 | As Figure 8 but for the phases of the AMM.

Overall, the atmospheric teleconnections between the Atl3 and renewable energy hubs are weak and spatially limited (Figures S6 and S9). As a result, the role of the Atl3 in complementarity is negligible.

Finally, Spearman correlation analysis confirms that interannual solar-wind complementarity is limited (a coefficient close to −1 implying high complementarity, Table S1). Most coefficients are positive or close to zero, indicating that co-variability is weak and often reinforcing rather than offsetting, consistent with the composite results in Figures 8 and 9.

5 | Discussion

There is substantial co-variability between the Atl3, AMM and ENSO due to shared atmospheric circulation patterns (Cai et al. 2019). In our analysis, specifically in boreal spring, the Atl3 and AMM phases behave like a seesaw (Figures 5 and 7, S1, S4, and S5). For instance, wind anomalies during the Atl3 negative phase resemble those of the AMM positive phase (Figures 5a,b and S4). The positive AMM is associated with cooling in the equatorial east Atlantic, a defining feature of the negative Atl3 (Vallès-Casanova et al. 2020). The southward cross-equatorial winds in the AMM negative phase have been proposed as a mechanism driving the development of the Atl3 positive phase in JJA (Foltz and McPhaden 2010), these winds strongly affect the eastern Brazil wind hub. Our results therefore suggest that impacts on wind and solar energy are more strongly linked to the AMM mechanisms than to east equatorial Atlantic variability (Atl3). The AMM is also influenced by ENSO (Casselman et al. 2022; García-Serrano et al. 2017), as seen in El Niño composites over the Caribbean SLP in MAM (Figure S6); however, further research is needed to clarify this connection. Two of the three energy hubs—the northern and eastern hubs—are particularly affected by the ENSO-AMM co-variability.

The impacts of El Niño and the Atl3 negative phase in JJA are similar, although the connection between the two modes is relatively weak (Lübbecke et al. 2018). In JJA, stronger eastern Atlantic trade winds are associated with the development of El Niño; the stronger winds enhance the Ekman pumping in the eastern equatorial Atlantic, producing the colder SSTAs related to the Atl3 negative phase (Figures S4 and S6). The same stronger winds extend over eastern Brazil during the Atl3 negative phase. The solar CF anomalies are similarly correlated with both modes (Figure S5 and 6g), but the mechanism is probably more related to the atmospheric subsidence and moisture divergence (Figure 6c), rather than to equatorial Atlantic cooling. In the case of the wind CF, the composites of the Atl3 are not significant. Moreover, some studies suggest a weakening of the Atl3 variability with future global warming due to ocean warming (Yang et al. 2022).

The impacts associated with the modes vary geographically with seasons, probably because the annual cycle of the ITCZ generates migration in the position of convergence, cloudiness and precipitation. In some cases, modes are seasonally locked (e.g., ENSO) (Timmermann et al. 2018).

Interannual complementarity between solar or wind energy within hubs is generally low, but opportunities may exist with hydropower (Gonzalez-Salazar and Poganietz 2021). Periods with weaker winds, greater cloudiness and reduced solar radiation may coincide with increased rainfall, enhancing water storage and hydropower generation (Figures 6 and 7). Conversely, drier periods bring higher solar radiation and are associated with stronger wind and energy production; for example, during El Niño in the three solar hubs (Figure 8a–c). The northern and western energy hubs are near the Andes where several hydropower dams already operate. Expansion of non-conventional renewable energy might stop the hydropower expansion in the Amazon, thereby reducing several environmental impacts, such as river ecology disruption and aquatic biodiversity loss (Chaudhari et al. 2021). Hydroclimate is not the only factor affecting hydropower variability; basin size, soils and topography also play a role (Ritter et al. 2020). Our analysis is limited to within-hub solar-wind complementarity; we do not assess inter-hub transmission constraints or implications for grid system-level reliability.

Predictability and complementarity are important for energy storage planning, whether in hydro-storage, gravitational or chemical batteries. Seasonal cycles (Figure 1) matter for long-term storage planning, whereas interannual anomalies are more important for monthly operations (Figures 8 and 9). Sub-seasonal predictability is key for complementarity. The pressure gradients associated with the ocean-atmospheric modes—shown in our results—could improve statistical forecasts, as SLP and SST variability are coupled in these modes. Thus, grid operators and energy planners could anticipate reduced renewable output or limited complementarity, based on improved seasonal forecasts of dominant climate modes such as ENSO and Atlantic variability. This will ensure a more reliable supply from combined sources and stored energy, thereby improving management of the grid. Power interconnections in the world and South America are affected by transnational regulatory and political issues; yet the north hub in Colombia and the northeast hub in Brazil have powerlines connecting both energy sources, and the connection between Perú and Bolivia is underdeveloped (EIA 2023). Assessments of scenarios of high voltage transmission lines remarked the great potential for covering the South American 2030 estimated demand (Barbosa et al. 2017; Plaza 2013). Day and night complementarity between solar and wind is necessary for operational (daily) management. The daily cloud cycle—morning versus afternoon convection—might impact solar energy; its evaluation requires considering small-scale meteorological processes, beyond the scope of our research.

Other climate phenomena may also affect renewable energy generation. Multidecadal oscillations influence atmospheric circulation, but their effect might be expressed in the dynamics of interannual modes. For instance, the Atlantic Multidecadal Oscillation, linked to aerosol forcing, might have influenced the AMM phases frequency (He et al. 2023); the Interdecadal Pacific Oscillation has also been associated with aerosol forcing (Qin et al. 2020). Other phenomena—at other time scales—also have impacts on renewables. Madden-Julian Oscillation changes the cloud cover and precipitation across South America (Alvarez et al. 2016; Fernandes and Grimm 2023), potentially influencing both solar and wind CF.

The impact of climate change on South American renewable energy remains uncertain. Some studies predict increases in wind and solar availability but reduced complementarity (de Souza Ferreira et al. 2024; Martinez and Iglesias 2024). Changes in the diurnal wind cycle are also possible. However, it is still debatable how climate change—either by GHG and/or aerosol emissions—will change the frequency, strength and teleconnections of the ocean-atmospheric modes (Wills et al. 2022), potentially reshaping how renewable energy variability is modulated.

Our results are underpinned by the homogeneous and physically consistent atmospheric interpolations (reanalysis), which represent regional circulation patterns and associated thermodynamics. The study omits fluctuations in efficiency due to turbine elements and electrical connections in both energy sources. Limitations also include dataset biases, but general atmospheric circulation is believed to be well represented (Hersbach et al. 2020). Nonetheless, the datasets are sufficiently robust to study interannual energy variability.

6 | Conclusions

This research advances the understanding of the ocean-atmospheric physical mechanisms linked to anomalies in potential renewable energy production. It also shows the possible complementarity between some renewable energy sources (wind and solar) and discusses options for balancing out meteorologically driven energy shortages. Our research identifies three regions of high climatological capacity factor (CF) in South America and focuses on the possible modulators of their variability. These energy hubs are: the North Caribbean, the Eastern Brazil and the Western Perú/Bolivia hub.

The interannual ocean-atmospheric modes act through a chain of processes:

- ENSO impacts: El Niño increases the wind CF in the northern Caribbean hub associated with negative SLP anomalies in the eastern equatorial Pacific, strengthening easterly Caribbean winds. It also boosts wind CF over northeast Brazil influenced by subsidence over the equatorial Atlantic, higher SLP and stronger trade winds. The descending motion also modulates the three solar hubs through associated anomalous moisture divergence and reduced cloud cover, which increases solar radiation. La Niña enhances convection and cloudiness, reducing the solar CF over tropical South America (particularly in the eastern hub). Moreover, in La Niña, the higher eastern Pacific SLP weakens the Caribbean trade winds, which reduces the northern hub wind CF.
- Atlantic modes of variability: both renewable sources are modulated by mechanisms of the AMM rather than the

changes in SLP and winds of the Atl3. The AMM is associated with cross-equatorial SLP and wind anomalies, which produce opposite impacts on the Caribbean and northeast Brazil wind hubs. It also influences the solar CF in eastern Brazil and Orinoco hubs via meridional moisture advection, which modulates moisture convergence, clouds and solar radiation depending on the phase of the mode. Impacts are asymmetric; for example, the solar CF in the eastern hub only responds during the AMM negative phase. The AMM impacts seem to migrate westward seasonally, while Atl3 impacts on continental energy variability are minimal.

Interannual complementarity of solar and wind energy is limited. Exceptions occur in SON in the northern hub for ENSO and AMM events and in JJA in the eastern and western hubs for AMM events. In most cases, both energy sources show anomalies of the same sign, but complementarity with hydropower is an alternative. Long-term planning of the eastern and western hubs must consider the low complementarity due to reduced availability between March and August for both energy sources.

Seasonal forecasts of energy production can be improved by considering the mechanisms studied in our research. Enhanced predictability of ENSO and Atlantic modes would help operators anticipate reduced renewable supply or weak complementarity and improve grid management. Considering short-scale phenomena is key for enhancing predictability and strengthening sub-seasonal to seasonal forecasts. Improved forecasts will enhance the resilience and sustainability of regional power systems.

Author Contributions

Nicolás Duque-Gardeazabal: conceptualization, data curation, formal analysis, funding acquisition, investigation, methodology, project administration, software, validation, writing – original draft, visualization, writing – review and editing. **Stefan Brönnimann:** conceptualization, funding acquisition, investigation, methodology, project administration, resources, supervision, validation, writing – review and editing. **Andrew R. Friedman:** data curation, investigation, methodology, writing – review and editing. **Edgar Dolores-Tesillos:** investigation, methodology, validation, writing – review and editing. **Olivia Martius:** methodology, writing – review and editing.

Acknowledgements

We are grateful to the institutions that gather and freely disseminate the data used in this research. N.D.-G. thanks Helena Gardeazabal, Joaquin Duque and friends for their emotional support throughout this research. Open access publishing facilitated by Universitat Bern, as part of the Wiley - Universitat Bern agreement via the Consortium of Swiss Academic Libraries.

Funding

N.D.-G. was supported by the Federal Commission for Scholarships for Foreign Students through the Swiss Government Excellence Scholarship (ESKAS No. 2022.0563) for the academic year(s) 2024–2025. A.R.F. was funded by the European Union's Horizon 2020 research and innovation program under the Marie Skłodowska-Curie grant No. 894064 (AQUATIC). Stefan Brönnimann was funded by the Swiss National Science Foundation (grant no. 10001375).

Data Availability Statement

Extended Reconstructed SST version 5 (Huang et al. 2017) is available at: https://www.ncei.noaa.gov/pub/data/cmb/ersst/v5/netcdf/. Mauna Loa CO_2 concentrations are available at https://gml.noaa.gov/ccgg/trends/data.html. ECMWF ERA5 reanalysis (Hersbach et al. 2020) data are available from Copernicus Climate Data Store web portal https://cds.climate.copernicus.eu. MSWEP (Beck et al. 2019) is available at: http://www.gloh2o.org/mswep/. EUMETSAT CLARA-A3 (Karlsson et al. 2023) is available at: https://wui.cmsaf.eu/safira/action/viewProduktDetails?fid=40&eid=22277_22492.

References

Alvarez, M. S., C. S. Vera, G. N. Kiladis, and B. Liebmann. 2016. "Influence of the Madden Julian Oscillation on Precipitation and Surface Air Temperature in South America." *Climate Dynamics* 46, no. 1–2: 245–262. https://doi.org/10.1007/s00382-015-2581-6.

Andrian, L. G., M. Osman, and C. S. Vera. 2024. "The Role of the Indian Ocean Dipole in Modulating the Austral Spring ENSO Teleconnection to the Southern Hemisphere." *Weather and Climate Dynamics* 5, no. 4: 1505–1522. https://doi.org/10.5194/wcd-5-1505-2024.

Antonini, E. G. A., E. Virgüez, S. Ashfaq, L. Duan, T. H. Ruggles, and K. Caldeira. 2024. "Identification of Reliable Locations for Wind Power Generation Through a Global Analysis of Wind Droughts." *Communications Earth & Environment* 5, no. 1: 1–9. https://doi.org/10.1038/s43247-024-01260-7.

Arango, S., and E. R. Larsen. 2010. "The Environmental Paradox in Generation: How South America Is Gradually Becoming More Dependent on Thermal Generation." *Renewable & Sustainable Energy Reviews* 14, no. 9: 2956–2965. https://doi.org/10.1016/j.rser.2010.07.049.

Arias, P. A., J. A. Martínez, J. D. Mejía, M. J. Pazos, J. C. Espinoza, and S. Wongchuig-Correa. 2020. "Changes in Normalized Difference Vegetation Index in the Orinoco and Amazon River Basins: Links to Tropical Atlantic Surface Temperatures." *Journal of Climate* 33, no. 19: 8537–8559. https://doi.org/10.1175/JCLI-D-19-0696.1.

Barbosa, L. d. S. N. S., D. Bogdanov, P. Vainikka, and C. Breyer. 2017. "Hydro, Wind and Solar Power as a Base for a 100% Renewable Energy Supply for South and Central America." *PLoS One* 12, no. 3: e0173820. https://doi.org/10.1371/journal.pone.0173820.

Beck, H. E., E. F. Wood, M. Pan, et al. 2019. "MSWEP V2 Global 3-Hourly 0.1° Precipitation: Methodology and Quantitative Assessment." *Bulletin of the American Meteorological Society* 100, no. 3: 473–500. https://doi.org/10.1175/BAMS-D-17-0138.1.

Bett, P. E., and H. E. Thornton. 2016. "The Climatological Relationships Between Wind and Solar Energy Supply in Britain." *Renewable Energy* 87: 96–110. https://doi.org/10.1016/j.renene.2015.10.006.

Bianchi, E., T. Guozden, and R. Kozulj. 2022. "Assessing Low Frequency Variations in Solar and Wind Power and Their Climatic Teleconnections." *Renewable Energy* 190: 560–571. https://doi.org/10.1016/j.renene.2022.03.080.

Bloomfield, H. C., D. J. Brayshaw, and A. J. Charlton-Perez. 2020. "Characterizing the Winter Meteorological Drivers of the European Electricity System Using Targeted Circulation Types." *Meteorological Applications* 27, no. 1: 1–18. https://doi.org/10.1002/met.1858.

Bloomfield, H. C., C. M. Wainwright, and N. Mitchell. 2022. "Characterizing the Variability and Meteorological Drivers of Wind Power and Solar Power Generation Over Africa." *Meteorological Applications* 29, no. 5: 2093. https://doi.org/10.1002/met.2093.

Boretti, A., and S. Castelletto. 2020. "Cost of Wind Energy Generation Should Include Energy Storage Allowance." *Scientific Reports* 10, no. 1: 2978. https://doi.org/10.1038/s41598-020-59936-x.

Bustos, C., D. Watts, and M. Ayala. 2017. “Financial Risk Reduction in Photovoltaic Projects Through Ocean-Atmospheric Oscillations Modeling.” *Renewable and Sustainable Energy Reviews* 74: 548–568. https://doi.org/10.1016/j.rser.2016.11.034.

Cai, W., M. J. McPhaden, A. M. Grimm, et al. 2020. “Climate Impacts of the El Niño–Southern Oscillation on South America.” *Nature Reviews Earth & Environment* 1, no. 4: 215–231. https://doi.org/10.1038/s43017-020-0040-3.

Cai, W., L. Wu, M. Lengaigne, et al. 2019. “Pantropical Climate Interactions.” *Science* 363: 4236. https://doi.org/10.1126/science.aav4236.

Cannon, D. J., D. J. Brayshaw, J. Methven, P. J. Coker, and D. Lenaghan. 2015. “Using Reanalysis Data to Quantify Extreme Wind Power Generation Statistics: A 33 Year Case Study in Great Britain.” *Renewable Energy* 75: 767–778. https://doi.org/10.1016/j.renene.2014.10.024.

Casselman, J. W., B. Jiménez-Esteve, and D. I. V. Domeisen. 2022. “Modulation of the El Niño Teleconnection to the North Atlantic by the Tropical North Atlantic During Boreal Spring and Summer.” *Weather and Climate Dynamics* 3, no. 3: 1077–1096. https://doi.org/10.5194/wcd-3-1077-2022.

Chaudhari, S., E. Brown, R. Quispe-Abad, E. Moran, N. Müller, and Y. Pokhrel. 2021. “In-Stream Turbines for Rethinking Hydropower Development in the Amazon Basin.” *Nature Sustainability* 4, no. 8: 680–687. https://doi.org/10.1038/s41893-021-00712-8.

Chiang, J. C. H., Y. Kushnir, and A. Giannini. 2002. “Deconstructing Atlantic Intertropical Convergence Zone Variability: Influence of the Local Cross-Equatorial Sea Surface Temperature Gradient and Remote Forcing From the Eastern Equatorial Pacific.” *Journal of Geophysical Research. Atmospheres* 107: 307. https://doi.org/10.1029/2000jd000307.

Compo, G. P., and P. D. Sardeshmukh. 2010. “Removing ENSO-Related Variations From the Climate Record.” *Journal of Climate* 23, no. 8: 1957–1978. https://doi.org/10.1175/2009JCLI2735.1.

de Perini Souza, N. B., J. V. dos Caro Santos, E. G. Sperandio Nascimento, A. A. Bandeira Santos, and D. M. Moreira. 2022. “Long-Range Correlations of the Wind Speed in a Northeast Region of Brazil.” *Energy* 243: 122742. https://doi.org/10.1016/j.energy.2021.122742.

de Souza Ferreira, G. W., M. S. Reboita, J. G. M. Ribeiro, et al. 2024. “Assessment of the Wind Power Density Over South America Simulated by CMIP6 Models in the Present and Future Climate.” *Climate Dynamics* 62, no. 3: 1729–1763. https://doi.org/10.1007/s00382-023-06993-3.

Dolores-Tesillos, E., N. Otero, and S. Allen. 2025. “Projections of Standardised Energy Indices in Future Climate Scenarios.” *Environmental Research Letters* 20, no. 1: 014026. https://doi.org/10.1088/1748-9326/ad9b3f.

Drumond, A., J. Marengo, T. Ambrizzi, R. Nieto, L. Moreira, and L. Gimeno. 2014. “The Role of the Amazon Basin Moisture in the Atmospheric Branch of the Hydrological Cycle: A Lagrangian Analysis.” *Hydrology and Earth System Sciences* 18, no. 7: 2577–2598. https://doi.org/10.5194/hess-18-2577-2014.

Duque-Gardeazabal, N., A. R. Friedman, and S. Brönnimann. 2025. “An Atlantic Influence on Evapotranspiration in the Orinoco and Amazon Basins.” *Hydrology and Earth System Sciences* 29, no. 14: 3277–3295. https://doi.org/10.5194/hess-29-3277-2025.

Eelsalu, M., R. D. Montoya, D. Aramburo, A. F. Osorio, and T. Soomere. 2024. “Spatial and Temporal Variability of Wave Energy Resource in the Eastern Pacific From Panama to the Drake Passage.” *Renewable Energy* 224: 120180. https://doi.org/10.1016/j.renene.2024.120180.

EIA. 2023. “Latin America Energy Outlook Interactive Map.” https://www.iea.org/data-and-statistics/data-tools/latin-america-energy-outlook-interactive-map.

Engeland, K., M. Borga, J. D. Creutin, B. François, M. H. Ramos, and J. P. Vidal. 2017. “Space-Time Variability of Climate Variables and Intermittent Renewable Electricity Production—A Review.” *Renewable & Sustainable Energy Reviews* 79: 600–617. https://doi.org/10.1016/j.rser.2017.05.046.

Evans, D. L., and L. W. Florschuetz. 1977. “Cost Studies on Terrestrial Photovoltaic Power Systems With Sunlight Concentration.” *Solar Energy* 19, no. 3: 255–262. https://doi.org/10.1016/0038-092X(77)90068-8.

Fernandes, K., A. Giannini, L. Verchot, W. Baethgen, and M. Pinedo-Vasquez. 2015. “Decadal Covariability of Atlantic SSTs and Western Amazon Dry-Season Hydroclimate in Observations and CMIP5 Simulations.” *Geophysical Research Letters* 42, no. 16: 6793–6801. https://doi.org/10.1002/2015GL063911.

Fernandes, L. G., and A. M. Grimm. 2023. “ENSO Modulation of Global MJO and Its Impacts on South America.” *Journal of Climate* 36: 1–48. https://doi.org/10.1175/jcli-d-22-0781.1.

Foltz, G. R., and M. J. McPhaden. 2010. “Interaction Between the Atlantic Meridional and Niño Modes.” *Geophysical Research Letters* 37, no. 18: 44001. https://doi.org/10.1029/2010GL044001.

García-Serrano, J., C. Cassou, H. Douville, A. Giannini, and F. J. Doblas-Reyes. 2017. “Revisiting the ENSO Teleconnection to the Tropical North Atlantic.” *Journal of Climate* 30, no. 17: 6945–6957. https://doi.org/10.1175/JCLI-D-16-0641.1.

Gil Ruiz, S. A., J. E. C. Barriga, and J. A. Martínez. 2021. “Wind Power Assessment in the Caribbean Region of Colombia, Using Ten-Minute Wind Observations and ERA5 Data.” *Renewable Energy* 172: 158–176. https://doi.org/10.1016/j.renene.2021.03.033.

Gonzalez-Salazar, M., and W. R. Poganietz. 2021. “Evaluating the Complementarity of Solar, Wind and Hydropower to Mitigate the Impact of El Niño Southern Oscillation in Latin America.” *Renewable Energy* 174: 453–467. https://doi.org/10.1016/j.renene.2021.04.048.

Gualtieri, G. 2022. “Analysing the Uncertainties of Reanalysis Data Used for Wind Resource Assessment: A Critical Review.” *Renewable & Sustainable Energy Reviews* 167: 112741. https://doi.org/10.1016/j.rser.2022.112741.

He, C., A. C. Clement, S. M. Kramer, et al. 2023. “Tropical Atlantic Multidecadal Variability Is Dominated by External Forcing.” *Nature* 622: 4. https://doi.org/10.1038/s41586-023-06489-4.

Henley, B. J., J. Gergis, D. J. Karoly, S. Power, J. Kennedy, and C. K. Folland. 2015. “A Tripole Index for the Interdecadal Pacific Oscillation.” *Climate Dynamics* 45: 3077–3090. https://doi.org/10.1007/s00382-015-2525-1.

Hersbach, H., B. Bell, P. Berrisford, et al. 2020. “The ERA5 Global Reanalysis.” *Quarterly Journal of the Royal Meteorological Society* 146, no. 730: 1999–2049. https://doi.org/10.1002/qj.3803.

Huang, B., P. W. Thorne, V. F. Banzon, et al. 2017. “Extended Reconstructed Sea Surface Temperature, Version 5 (ERSSTv5): Upgrades, Validations, and Intercomparisons.” *Journal of Climate* 30, no. 20: 8179–8205. https://doi.org/10.1175/JCLI-D-16-0836.1.

Karlsson, K.-G., A. Riihelä, J. Trentmann, et al. 2023. “CLARA-A3: CM SAF Cloud, Albedo and Surface RAdiation Dataset From AVHRR Data—Edition 3. Satellite Application Facility on Climate Monitoring (CM SAF).” https://doi.org/10.5676/EUM_SAF_CM/CLARA_AVHRR/V003.

Kieffer, G., and Á. López-Peña. 2016. *Renewable Energy Market Analysis: Latin America*. International Renewable Energy Agency.

Kies, A., B. U. Schyska, M. Bilousova, O. El Sayed, J. Jurasz, and H. Stoecker. 2021. “Critical Review of Renewable Generation Datasets and Their Implications for European Power System Models.” *Renewable and Sustainable Energy Reviews* 152: 111614. https://doi.org/10.1016/j.rser.2021.111614.

Lopes, A. V., J. C. H. Chiang, S. A. Thompson, and J. A. Dracup. 2016. “Trend and Uncertainty in Spatial-Temporal Patterns of Hydrological Droughts in the Amazon Basin.” *Geophysical Research Letters* 43, no. 7: 3307–3316. https://doi.org/10.1002/2016GL067738.

Lübbecke, J. F., B. Rodríguez-Fonseca, I. Richter, et al. 2018. "Equatorial Atlantic Variability—Modes, Mechanisms, and Global Teleconnections." *WIREs Climate Change* 9, no. 4: 1–18. https://doi.org/10.1002/wcc.527.

Martinez, A., and G. Iglesias. 2024. "Climate Change and Wind Energy Potential in South America." *Science of the Total Environment* 957: 177675. https://doi.org/10.1016/j.scitotenv.2024.177675.

Martín-Rey, M., B. Rodríguez-Fonseca, I. Polo, and F. Kucharski. 2014. "On the Atlantic–Pacific Niños Connection: A Multidecadal Modulated Mode." *Climate Dynamics* 43, no. 11: 3163–3178. https://doi.org/10.1007/s00382-014-2305-3.

Otero, N., O. Martius, S. Allen, H. Bloomfield, and B. Schaefli. 2022. "A Copula-Based Assessment of Renewable Energy Droughts Across Europe." *Renewable Energy* 201: 667–677. https://doi.org/10.1016/j.renene.2022.10.091.

Pabón, J. D., and J. Dorado. 2008. "INTRASEASONAL Variability of Rainfall Over Northern South America and Caribbean Region." *Earth Sciences Research Journal* 12, no. 2: 194–212.

Plaza, R. M. 2013. "Transnational Power Transmission and International Law." *International Review of Law* 2013, no. 2: 8. https://doi.org/10.5339/irl.2013.8.

Qin, M., A. Dai, and W. Hua. 2020. "Aerosol-Forced Multidecadal Variations Across All Ocean Basins in Models and Observations Since 1920." *Science Advances* 6, no. 29: 1–8. https://doi.org/10.1126/sciadv.abb0425.

Ramirez Camargo, L., and J. Schmidt. 2020. "Simulation of Multi-Annual Time Series of Solar Photovoltaic Power: Is the ERA5-Land Reanalysis the Next Big Step?" *Sustainable Energy Technologies and Assessments* 42: 100829. https://doi.org/10.1016/j.seta.2020.100829.

Ritter, J., G. Corzo, D. P. Solomatine, and H. Angarita. 2020. "Multiobjective Direct Policy Search Using Physically Based Operating Rules in Multireservoir Systems." *Journal of Water Resources Planning and Management* 146, no. 4: 1159. https://doi.org/10.1061/(ASCE)WR.1943-5452.0001159.

Ruiz-Barradas, A., J. A. Carton, and S. Nigam. 2000. "Structure of Interannual-To-Decadal Climate Variability in the Tropical Atlantic Sector." *Journal of Climate* 13, no. 18: 3285–3297.

Sianturi, Y., Y. Marjuki, and K. Sartika. 2020. "Evaluation of ERA5 and MERRA2 Reanalyses to Estimate Solar Irradiance Using Ground Observations Over Indonesia Region." In *AIP Conference Proceedings*, 020002. AIP Publishing LLC. https://doi.org/10.1063/5.0000854.

Thoning, K. W., P. P. Tans, and W. D. Komhyr. 1989. "Atmospheric Carbon Dioxide at Mauna Loa Observatory: 2. Analysis of the NOAA GMCC Data, 1974-1985." *Journal of Geophysical Research: Atmospheres* 94, no. D6: 8549–8565. https://doi.org/10.1029/JD094iD06p08549.

Timmermann, A., S. I. An, J. S. Kug, et al. 2018. "El Niño–Southern Oscillation Complexity." *Nature* 559, no. 7715: 535–545. https://doi.org/10.1038/s41586-018-0252-6.

Towner, J., A. Ficchí, H. L. Cloke, J. Bazo, E. Coughlan de Perez, and E. M. Stephens. 2021. "Influence of ENSO and Tropical Atlantic Climate Variability on Flood Characteristics in the Amazon Basin." *Hydrology and Earth System Sciences* 25, no. 7: 3875–3895. https://doi.org/10.5194/hess-25-3875-2021.

UN. 2015. "Transforming Our World: The 2030 Agenda for Sustainable Development." https://documents.un.org/doc/undoc/gen/n15/291/89/pdf/n1529189.pdf.

Vallès-Casanova, I., S. Lee, G. R. Foltz, and J. L. Pelegrí. 2020. "On the Spatiotemporal Diversity of Atlantic Niño and Associated Rainfall Variability Over West Africa and South America." *Geophysical Research Letters* 47, no. 8: 1–10. https://doi.org/10.1029/2020GL087108.

Vargas Gil, G. M., R. Bittencourt Aguiar Cunha, S. Giuseppe Di Santo, R. Machado Monaro, F. Fragoso Costa, and A. J. Sguarezi Filho. 2020. "Photovoltaic Energy in South America: Current State and Grid Regulation for Large-Scale and Distributed Photovoltaic Systems." *Renewable Energy* 162: 1307–1320. https://doi.org/10.1016/j.renene.2020.08.022.

Wilczak, J. M., E. Akish, A. Capotondi, and G. P. Compo. 2024. "Evaluation and Bias Correction of the ERA5 Reanalysis Over the United States for Wind and Solar Energy Applications." *Energies* 17, no. 7: 1667. https://doi.org/10.3390/en17071667.

Williams, I. N., and C. M. Patricola. 2018. "Diversity of ENSO Events Unified by Convective Threshold Sea Surface Temperature: A Nonlinear ENSO Index." *Geophysical Research Letters* 45, no. 17: 9236–9244. https://doi.org/10.1029/2018GL079203.

Wills, R. C. J., Y. Dong, C. Proistosecu, K. C. Armour, and D. S. Battisti. 2022. "Systematic Climate Model Biases in the Large-Scale Patterns of Recent Sea-Surface Temperature and Sea-Level Pressure Change." *Geophysical Research Letters* 49, no. 17: 11. https://doi.org/10.1029/2022GL100011.

Wind-turbine-models. 2025. "Vestas V117-3.45." https://en.wind-turbine-models.com/turbines/1248-vestas-v117-3.45#powercurve.

Yang, Y., L. Wu, W. Cai, et al. 2022. "Suppressed Atlantic Niño/Niña Variability Under Greenhouse Warming." *Nature Climate Change* 12, no. 9: 814–821. https://doi.org/10.1038/s41558-022-01444-z.

Supporting Information

Additional supporting information can be found online in the Supporting Information section. **Data S1:** met70165-sup-0001-Supinfo.docx.